SPICE-Compatible Models for Multiconductor Transmission Lines in Laplace-Transform Domain

Antonije R. Djordjević

***Abstract*— Two models for multiconductor transmission lines are presented that are compatible with SPICE. One model is based on a Thévenin equivalent circuit and the other model is based on mode decoupling. The models contain controlled generators in the Laplace-transform domain and are able to handle lossy lines with frequency-dependent parameters.**

***Index Terms*—Multiconductor transmission lines.**

I. Introduction

MOST DIGITAL circuits and some microwave circuits contain multiconductor transmission lines (e.g., computer buses, some directive couplers, and filters). In spite of this, most popular computer-aided design (CAD) programs still do not include arbitrary multiconductor lines as standard elements. In particular, many digital-circuit designers and microwave engineers use various versions of the program known under the generic name SPICE. In recent releases [1], this program has a built-in model only for a simple transmission line. In subcircuit libraries, it has an obsolete lumped-element model for a simple line and models for 2–5 coupled lines. The latter models are rather incomplete. They assume the lines to have identical parameters, which is questionable in both theory and practice. The models take into account the coupling only between adjacent lines, which is of a limited use. In all cases, the lines can be either lossless or lossy. However, the primary parameters are independent of frequency. This is insufficient for many applications, as the losses are most often frequency-dependent.

There exists much literature which deals with the analysis of the frequency-domain and time-domain responses of multiconductor lines. However, very few of them [2]–[4] describe theoretically well-founded SPICE-compatible models for multiconductor transmission lines. A model for lossless lines (with frequency-independent primary matrix parameters) is presented in [2]. The model is a subcircuit prototype that involves controlled generators and simple transmission lines. Although this model works fine in many cases, there are some computational problems, as explained in Section IV. The model described in [3] is an improvement of the previous model. It works well for arbitrary lines and it has been designed to be compatible with virtually any technique for the electromagnetic-field analysis of multiconductor transmission lines. However, this model is restricted to lossless lines. A model that includes frequency-dependent losses and dispersion is described in [4]. In this model, the dispersive modal propagation is emulated by ladder networks of lumped elements, which may result in huge circuits if long transmission lines are analyzed.

None of these models can efficiently model multiconductor transmission lines with frequency-dependent losses. This paper is aimed at presenting two novel SPICE-compatible models that can perform such a task. The first model, described in Section II, is based on a Thévenin equivalent circuit. It utilizes controlled generators in the Laplace-transform domain to model the modal delay, attenuation due to losses, and dispersion. Particular care is taken to provide causal responses in the time domain, as explained in Section III. The second model, described in Section IV, is a hybrid between the model of Section II and the model of [3]. Finally, several examples of the analysis using the proposed models are presented in Section V, together with experimental data.

Both models presented in this paper are subcircuit prototypes that can easily be included into SPICE or other similar programs [5].

Assume the multiconductor transmission lines to have a total of $(N+1)$ signal conductors. The first N conductors are referred to as the signal conductors. The last conductor is the reference conductor (although in practice it can be "floating"). The line can guide TEM, quasi-TEM, or hybrid waves, but it is assumed that the state on the line can be adequately described by voltages and currents. Details on the analysis of the transmission-line response are avoided, as they can be found in [6]–[8].

II. Thévenin Equivalent-Circuit Model

Let the x-axis be oriented along the length of the line, with $x = 0$ corresponding to end #1 of the line ("generator" end), and $x = D$ $(D > 0)$ to end #2 of the line ("load" end). The transmission line is assumed to be terminated at each end in a network, which is referred to as the terminal network. The basic circuit-theory equations describing such a line in the

Manuscript received September 29, 1995; revised December 24, 1996. This work was supported in part by the Serbian Ministry of Science and Technology.

A. R. Djordjević is with the University of Belgrade, School of Electrical Engineering, 11001 Belgrade, Yugoslavia.

Publisher Item Identifier S 0018-9480(97)02533-7.

Laplace-transform domain are the telegraphers' equations

$$\frac{d[\mathbf{V}(x)]}{dx} = -[\mathbf{R}][\mathbf{I}(x)] - s[\mathbf{L}][\mathbf{I}(x)], \quad 0 < x < D \tag{1}$$

$$\frac{d[\mathbf{I}(x)]}{dx} = -[\mathbf{G}][\mathbf{V}(x)] - s[\mathbf{C}][\mathbf{V}(x)], \quad 0 < x < D \tag{2}$$

where $[\mathbf{V}(x)]$ is a vector of complex voltages between the signal conductors and the reference conductor at position x along the line, $[\mathbf{I}(x)]$ is the corresponding vector of complex currents of the signal conductors, $[\mathbf{R}]$, $[\mathbf{L}]$, $[\mathbf{C}]$, and $[\mathbf{G}]$ are the primary matrix parameters of the line, and s is the complex frequency ($s = j\omega$ on the imaginary axis, where $\omega = 2\pi f$ is the angular frequency, and f is the frequency). The general solution of the telegraphers' equations can be obtained by expanding the line state in terms of modes whose propagation along the line is expressed by a multiplicative factor of the form $\exp(\mp\gamma_i x)$ where $\gamma_i = \alpha_i + j\beta_i$ is the modal propagation coefficient ($i = 1, \cdots, N$). The line voltages and currents can be expressed in terms of the modes as

$$\begin{aligned}[\mathbf{V}(x)] &= [\mathbf{V}_{\text{inc}}(x)] + [\mathbf{V}_{\text{ref}}(x)] \\ &= [\mathbf{S}_V]\{[\mathbf{G}_{\text{inc}}(x)] + [\mathbf{G}_{\text{ref}}(x)]\}\end{aligned} \tag{3}$$

$$\begin{aligned}[\mathbf{I}(x)] &= [\mathbf{I}_{\text{inc}}(x)] + [\mathbf{I}_{\text{ref}}(x)] \\ &= [\mathbf{S}_I]\{[\mathbf{G}_{\text{inc}}(x)] - [\mathbf{G}_{\text{ref}}(x)]\}\end{aligned} \tag{4}$$

where the indices "inc" and "ref" correspond to the waves traveling in the direction of the x-axis and in the opposite direction, respectively, $[\mathbf{G}_{\text{inc}}(x)]$ and $[\mathbf{G}_{\text{ref}}(x)]$ are vectors of modal intensities, $[\mathbf{S}_V]$ is the modal voltage matrix, and $[\mathbf{S}_I]$ the modal current matrix. The modal matrices and the characteristic impedance matrix are related by

$$[\mathbf{Z}_c] = [\mathbf{S}_V][\mathbf{S}_I]^{-1} = [\mathbf{S}_V][\Gamma]^{-1}[\mathbf{S}_V]^{-1}([\mathbf{R}] + s[\mathbf{L}]) \tag{5}$$

where $[\Gamma] = \text{diag}(\gamma_1 \cdots \gamma_N)$. The modal intensities at the two line ends are related by

$$[\mathbf{G}_{\text{inc}}(D)] = [\mathbf{E}][\mathbf{G}_{\text{inc}}(0)] \tag{6}$$

$$[\mathbf{G}_{\text{ref}}(0)] = [\mathbf{E}][\mathbf{G}_{\text{ref}}(D)] \tag{7}$$

where $[\mathbf{E} = \text{diag}[\exp(-\gamma_i D) \cdots \exp(-\gamma_N D)]$. Now,

$$[\mathbf{V}(0)] = [\mathbf{S}_V]\{[\mathbf{G}_{\text{inc}}(0)] + [\mathbf{E}][\mathbf{G}_{\text{ref}}(D)]\} \tag{8}$$

$$[\mathbf{I}(0)] = [\mathbf{S}_I]\{[\mathbf{G}_{\text{inc}}(0)] - [\mathbf{E}][\mathbf{G}_{\text{ref}}(D)]\} \tag{9}$$

$$[\mathbf{V}(D)] = [\mathbf{S}_V]\{[\mathbf{E}][\mathbf{G}_{\text{inc}}(0)] + [\mathbf{G}_{\text{ref}}(D)]\} \tag{10}$$

$$[\mathbf{I}(D)] = [\mathbf{S}_I]\{[\mathbf{E}][\mathbf{G}_{\text{inc}}(0)] - [\mathbf{G}_{\text{ref}}(D)]\}. \tag{11}$$

Equation (9) can be multiplied $[\mathbf{Z}_c]$ by and subtracted from (8). Taking (5) into account, one obtains

$$\begin{aligned}[\mathbf{V}(0)] - [\mathbf{Z}_c][\mathbf{I}(0)] &= 2[\mathbf{S}_V][\mathbf{E}][\mathbf{G}_{\text{ref}}(D)] \\ &= 2[\mathbf{S}_V][\mathbf{G}_{\text{ref}}(0)] = 2[\mathbf{V}_{\text{ref}}(0)]\end{aligned} \tag{12}$$

which defines the Thévenin equivalent circuit looking into end #1 of the line (Fig. 1). The passive portion of this circuit has the same impedance matrix as the characteristic impedance matrix of the multiconductor transmission line. The electromotive forces are related to the intensities of the modes traveling in the direction of the negative x-axis. The vector $[\mathbf{E}][\mathbf{G}_{\text{ref}}(D)]$ represents the intensities of modes launched from end #2 and propagated all the way to end #1. A similar derivation can be carried out starting from (10) and (11) to yield a relation between the voltage and current vectors for end #2, which defines the Thévenin equivalent circuit looking into this end (Fig. 1).

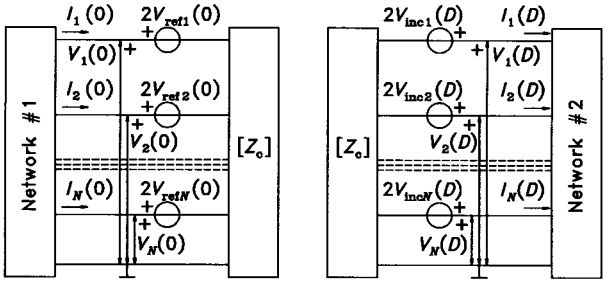

Fig. 1. The Thévenin equivalent circuit for a multiconductor transmission line.

Considering this circuit, one is able design the first SPICE-compatible model, shown in Fig. 2. For simplicity, the model is shown for $N = 3$. Each passive network (with the impedance matrix $[\mathbf{Z}_c]$) can be synthesized as a complete N-polygon with parallel branches to ground. The admittances of the branches of this network can be expressed in terms of the elements of the characteristic admittance matrix $[\mathbf{Y}_c] = [\mathbf{Z}_c]^{-1}$. For a lossless and dispersionless line, this network is purely resistive. For a lossy and dispersive line, the admittances are complex and frequency-dependent. However, in many practical cases, the influence of the line losses on the characteristic admittance matrix and the modal patterns is relatively small. To simplify the analysis, the elements of the characteristic admittance matrix, as well as of the modal voltage and current matrices, may be taken to be real and frequency-independent.

The electromotive forces of the Thévenin equivalent circuit for each line end are emulated by N-controlled voltage generators, located at the very left and right ends of the scheme of Fig. 2. Each generator is controlled by N modal intensities. According to (12), each multiplicative factor equals twice the corresponding element of the modal voltage matrix.

The intensities of propagated modes are represented in the circuit by electromotive forces of controlled voltage generators in the Laplace-transform domain, located in the middle of the circuit of Fig. 2. (To conform to SPICE circuit restrictions, these generators must not be left open. They can be terminated by arbitrary resistors, not shown in Fig. 2.) The propagation of a mode is taken into account by the multiplicative exponential factor of the form $\exp(-\gamma D)$ in the control function for a generator, thus emulating (6) and (7). This factor multiplies the intensity of the mode launched from the other transmission-line end. The intensity of the launched mode is evaluated from the voltages at the corresponding line end and the intensities of modes incident on that end. For end #1, according to (8), one has

$$\begin{aligned}[\mathbf{G}_{\text{inc}}(0)] &= [\mathbf{S}_V]^{-1}[\mathbf{V}(0)] - [\mathbf{E}][\mathbf{G}_{\text{ref}}(D)] \\ &= [\mathbf{S}_V]^{-1}[\mathbf{V}(0)] - [\mathbf{G}_{\text{ref}}(0)]\end{aligned} \tag{13}$$

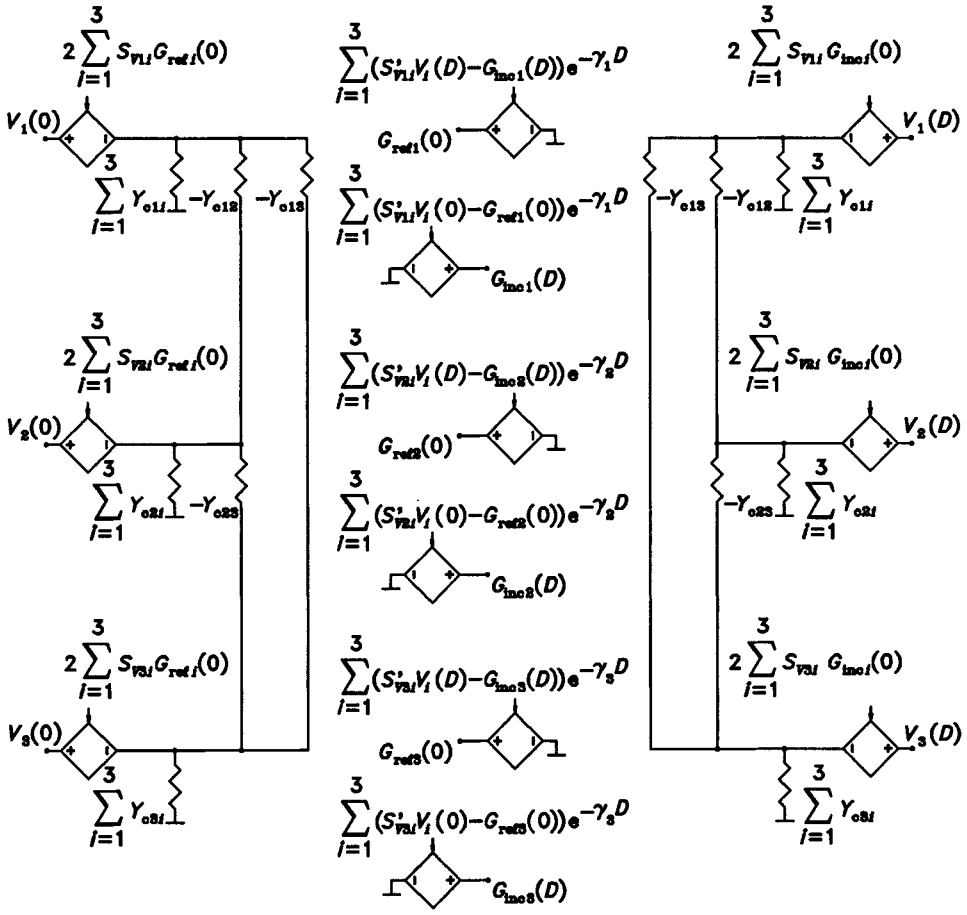

Fig. 2. A SPICE-compatable model based on the Thévenin equivalent circuit for $N = 3$.

and a similar relation can be written for end #2. In the model of Fig. 2, S'_{Vij} denotes the elements of the matrix $[\mathbf{S}_V]^{-1}$.

For the frequency-domain analysis, the Laplace transform is easily incorporated into the analysis. For the time-domain analysis, however, SPICE must first evaluate the inverse Laplace transform (i.e., the pulse response) for each exponential factor and then convolve it with the controlling voltages at each time step.

III. Causality of the Response

In the evaluation of the time-domain response (in particular for long lines) the frequency variations and the complex character of the modal propagation coefficients must be properly taken into account. This can be achieved by fitting the results of an electromagnetic analysis of the line, which includes the line losses and dispersion. Thereby, special care should be taken to obtain a causal response [9]. Considering the analogy with a simple line, the author will present here some simple equations for the modal propagation coefficients that satisfy the causality requirements.

The real part of each modal propagation coefficient $\alpha_i\,(i = 1, \cdots, N)$ can be approximately separated into two parts as $\alpha_i = \alpha_{ci} + \alpha_{di}$, where α_{ci} is due to the conductor losses and α_{di} is due to the dielectric losses. In practical cases, the matrix $[\mathbf{G}]$ has a negligible influence on α_{ci} and the matrix $[\mathbf{R}]$ has a negligible influence on α_{di}. Hence, for a lossy line, two modal analyses can be performed (for example, at a reference frequency, f_{ref}). First, take $[\mathbf{G}] = 0$ and evaluate α_{ci} for all modes. Second, take $[\mathbf{R}] = 0$ and evaluate α_{di}. However, the attenuation coefficients α_{ci} and α_{di} usually strongly depend on frequency. The actual variations of the matrices $[\mathbf{R}]$ and $[\mathbf{G}]$ are complicated and depend on the properties of the conductor and dielectric materials involved in constructing the line. For example, for normal conductors in the skin-effect region $[\mathbf{R}]$ and α_{ci} are approximately proportional to the square root of frequency, and for superconductors, to frequency squared. For poor dielectrics where the conductive losses dominate, the matrix $[\mathbf{G}]$ is independent of frequency and α_{di} is also constant. For good dielectrics at microwave frequencies, the electron polarization dominates and $[\mathbf{G}]$ and α_{di} are approximately proportional to frequency squared (corresponding to a loss tangent that linearly increases with frequency). However, except when both α_{ci} and α_{di} are independent of frequency, the resulting time-domain response will not be causal unless appropriate frequency variations of the modal phase coefficients or, equivalently, of the modal phase velocities ($c_{\phi i}$), are taken into account.

Consider a simple transmission line. Its propagation coefficient is given in the Laplace-transform domain by

$$\gamma(s) = \sqrt{(R(s) + sL(s))(G(s) + sC(s))} \qquad (14)$$

where R, L, G, and C are the primary (scalar) parameters of the line, which generally depend on s. Equation (14) can be rearranged as (15) as shown at the bottom of the following page, where for $s = j\omega$, $a(s) \approx \alpha_c$, $b(s) \approx \alpha_d$, $c(s) \approx c_\phi$, and $A(s)$ and $B(s)$ denote the corresponding factors in brackets.

In the simplest case of a lossless simple line (with frequency-independent parameters)

$$A(s) = B(s) = \frac{s}{c_\phi(s_{\rm ref})} \tag{16}$$

where $s_{\rm ref} = 2j\pi f_{\rm ref}$. Such a line can be approximated in the circuit theory by a ladder network that consists of frequency-independent inductors in series branches and capacitors in parallel branches. Naturally, its response is causal, and (16) presents the simplest cases of $A(s)$ and $B(s)$ that yield a causal response.

If a lossy simple transmission line has frequency-independent parameters (which in practice corresponds to lower frequencies, where the skin effect is not pronounced), then $a(s)$, $b(s)$, and $c(s)$ are independent of frequency, so that $A(s)$ and $B(s)$ are given by

$$A(s) = 2\alpha_c(s_{\rm ref}) + \frac{s}{c_\phi(s_{\rm ref})} \tag{17}$$

and

$$B(s) = 2\alpha_d(s_{\rm ref}) + \frac{s}{c_\phi(s_{\rm ref})}. \tag{18}$$

Such a line also has a causal response. Following the approach in [4], the line can be approximated by a ladder network consisting of frequency-independent inductors and resistors (connected in series) in series branches, and capacitors and resistors (connected in parallel) in parallel branches.

If the skin effect is fully pronounced on a simple line, then $R(s) = R(s_{\rm ref})\sqrt{s/s_{\rm ref}}$ and $sL(s) = sL_e + sL_i(s) = sL_e + R(s)$, where L_e is the per-unit-length external inductance (which is frequency-independent) and L_i is the per-unit-length internal inductance (which is inversely proportional to $\sqrt{s}$). In this case, $a(s)$ is practically proportional to the square root of frequency, and the inductance has a small frequency-dependent term. Hence,

$$A(s) = 2\alpha_c(s_{\rm ref})\sqrt{\frac{2js}{s_{\rm ref}}} + \frac{s}{c_\phi(s_{\rm ref})} \tag{19}$$

is the third example of $A(s)$ that gives a causal response.

Finally, one can consider a simple lossy line with a dielectric loss tangent that is approximately a linear function of frequency. If the line conductors are assumed to be lossless, the line can be approximated by a ladder network of frequency-independent inductors in series branches and capacitors and resistors (connected in series) in parallel branches. Hence, the equivalent capacitance per-unit length of this line slightly varies with frequency, and the conductance is proportional to frequency squared. The response of such a line is also causal, thus having

$$B(s) = \frac{1}{2\alpha_d(s_{\rm ref})\left(\frac{jc_\phi(s_{\rm ref})}{s_{\rm ref}}\right)^2 + \frac{c_\phi(s_{\rm ref})}{s}}. \tag{20}$$

A similar procedure can be done for superconductors ($r = 2$). To obtain a causal response, one can combine any pair of $A(s)$ and $B(s)$ from (16) to (20).

In order to secure a causal response for a multiconductor transmission line, take (15) (at the bottom of the page) to express each modal propagation coefficient (γ_i) in terms of $A(s)$ and $B(s)$ that are related to the corresponding modal attenuation coefficients (α_{ci} and α_{di}) and the modal phase velocity ($c_{\phi i}$) by (16)–(20). Thereby, the modal analysis is performed only at the reference frequency, which can be chosen arbitrarily, and (16)–(20) is selected based on the assumed frequency variations of losses.

IV. Modal Decomposition Model

The derivation of the second SPICE-compatible model is based on the model described in [3], which can be considered as an improvement of the model of [2]. The model of [3] can be derived starting from telegraphers' equations in the frequency domain (although a similar procedure can be performed in the time domain). Substituting (3) and (4) into (1) and (2), yields

$$\frac{d}{dx}\{[\mathbf{G}_{\rm inc}(x)] + [\mathbf{G}_{\rm ref}(x)]\} = -[\Gamma]\{[\mathbf{G}_{\rm inc}(x)] - [\mathbf{G}_{\rm ref}(x)]\} \tag{21}$$

$$\frac{d}{dx}\{[\mathbf{G}_{\rm inc}(x)] - [\mathbf{G}_{\rm ref}(x)]\} = -[\Gamma]\{[\mathbf{G}_{\rm inc}(x)] + [\mathbf{G}_{\rm ref}(x)]\}. \tag{22}$$

Equations (21) and (22) can be interpreted as telegraphers' equations for a virtual multiconductor transmission line where the element $G_{{\rm inc}m}(x)$ of the vector $[\mathbf{G}_{\rm inc}(x)]$ is the voltage of the incident wave on conductor m, and the element $G_{{\rm ref}m}(x)$ of $[\mathbf{G}_{\rm ref}(x)]$ is the voltage of the reflected wave. However, since the matrix $[\Gamma]$ is diagonal, the signal conductors of this line are decoupled, and (21) and (22) can be written in scalar form as

$$\frac{d}{dx}(G_{{\rm inc}m}(x) + G_{{\rm ref}m}(x)) = -\gamma_m(G_{{\rm inc}m}(x) - G_{{\rm ref}m}(x)), \quad m = 1, \cdots, N \tag{23}$$

$$\frac{d}{dx}(G_{{\rm inc}m}(x) - G_{{\rm ref}m}(x)) = -\gamma_m(G_{{\rm inc}m}(x) + G_{{\rm ref}m}(x)), \quad m = 1, \cdots, N. \tag{24}$$

$$\gamma(s) = \sqrt{\left(\frac{R(s)}{\sqrt{L(s)/C(s)}} + s\sqrt{L(s)C(s)}\right)\left(\frac{G(s)}{\sqrt{C(s)/L(s)}} + s\sqrt{L(s)C(s)}\right)}$$
$$= \sqrt{\left(2a(s) + \frac{s}{c(s)}\right)\left(2b(s) + \frac{s}{c(s)}\right)} = \sqrt{A(s)B(s)} \tag{15}$$

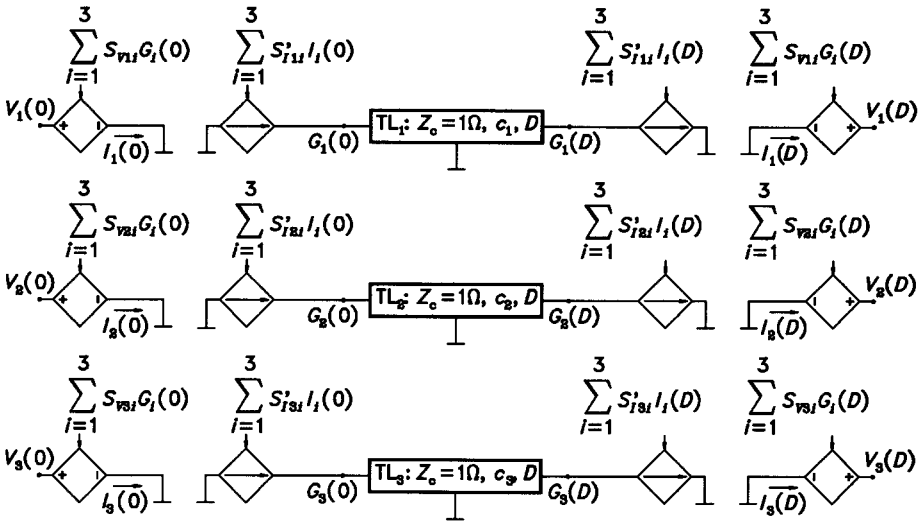

Fig. 3. A SPICE-compatible model for lossless lines based on the modal decoupling for $N = 3$. (Reprinted from [3].)

A pair of the above equations (for the same m) describes a simple transmission line of characteristic impedance $Z_{cm} = 1$ (no units) and propagation coefficient $\gamma_m \cdot G_{\text{inc}m}(x)$ can also be interpreted as the current of the incident wave of the conductor m, and $-G_{\text{ref}m}(x)$ as the current of the reflected wave. From (3) and (4), the actual voltages and currents at the original multiconductor transmission-line terminals are related to the voltages and currents of the virtual (decoupled) line by

$$[\mathbf{V}(0)] = [\mathbf{S}_V]\{[\mathbf{G}_{\text{inc}}(0)] + [\mathbf{G}_{\text{ref}}(0)]\} \quad (25)$$

$$\{[\mathbf{G}_{\text{inc}}(0)] - [\mathbf{G}_{\text{ref}}(0)]\} = [\mathbf{S}_I]^{-1}[\mathbf{I}(0)] \quad (26)$$

$$[\mathbf{V}(D)] = [\mathbf{S}_V]\{[\mathbf{G}_{\text{inc}}(D)] + [\mathbf{G}_{\text{ref}}(D)]\} \quad (27)$$

$$\{[\mathbf{G}_{\text{inc}}(D)] - [\mathbf{G}_{\text{ref}}(D)]\} = [\mathbf{S}_I]^{-1}[\mathbf{I}(D)]. \quad (28)$$

Equations (25) and (27) can be emulated in SPICE by controlled voltage generators, and (26) and (28) by controlled current generators. For a lossless multiconductor transmission line, a SPICE-compatible model can be designed [3] as shown in Fig. 3 (for $N = 3$). Each simple transmission line in that model is lossless, its characteristic impedance is 1 Ω, the length is D, while the wave propagation velocity along the line (c_i) equals the corresponding modal phase velocity and is assumed to be independent of frequency, which is the only case that can be directly modeled by SPICE. Note that in [3] a different definition of the characteristic impedances is used, which is incompatible with (5). In Fig. 3, S'_{Iij} denotes the elements of the matrix $[\mathbf{S}_I]^{-1}$. All controlled generators in Fig. 3 are ordinary (i.e., not in the Laplace-transform domain). The control functions for the voltage generators include voltages at the terminals of the simple transmission lines and their inclusion into the SPICE model is straightforward. However, the control functions for the current generators include currents at the terminals of the subcircuit. In order to sample these currents, dummy independent voltage generators (of zero electromotive force) have to be added in series with the controlled voltage generators (not shown in Fig. 3). The currents of these dummy generators are used to control the current generators.

At this point, some advantages of the model of [3] (Fig. 3) over the model of [2] should be stressed, which are transferred to the model that will be developed later in this section. First, the model of Fig. 3 accepts an arbitrary modal voltage matrix $[\mathbf{S}_V]$, while for the model of [2] this matrix must be normalized so to satisfy the condition $([\mathbf{S}_V]^t)^{-1} = [\mathbf{S}_I]$, where the superscript "t" denotes transpose. This normalization may be inconvenient for several reasons. First, when the eigenvalue analysis of the line is performed many standard computer programs for this purpose do not yield the required normalization. A similar situation may occur if the modes are evaluated directly from an electromagnetic-field analysis (e.g., from a full-wave solution of the line). In both cases, an additional computational effort is required to reduce the matrix $[\mathbf{S}_V]$ to the required form. Another problem for the model of [2] occurs when the modes are degenerate (for a lossless multiconductor transmission line in a homogeneous dielectric), when the modal analysis can result in an arbitrary (regular) matrix $[\mathbf{S}_V]$, and even more computational effort is required to properly normalize this matrix. In this case, the model of Fig. 3 can accept an arbitrary matrix $[\mathbf{S}_V]$, even the simplest case of a unit matrix, and the corresponding matrix $[\mathbf{S}_I]$ is evaluated from (5).

Second, the characteristics of modes may not be evaluated from the primary matrix parameters, but rather from an electromagnetic-field analysis. The model of Fig. 3 requires knowing only the modal propagation coefficients and the two modal matrices ($[\mathbf{S}_V]$ and $[\mathbf{S}_I]$), which is compatible with many techniques for the electromagnetic-field analysis of multiconductor lines, including the full-wave analysis. The model of [2] requires knowing the primary matrix parameters from which the modal propagation coefficients, the matrices $[\mathbf{S}_V]$ and $[\mathbf{S}_I]$, and the characteristic impedances of the decoupled simple transmission lines have to be calculated. In cases when the primary matrix parameters are not evaluated by the field analysis, the model of [2] requires an additional effort to identify the characteristic impedances of the simple transmission lines, which makes it harder to be applied.

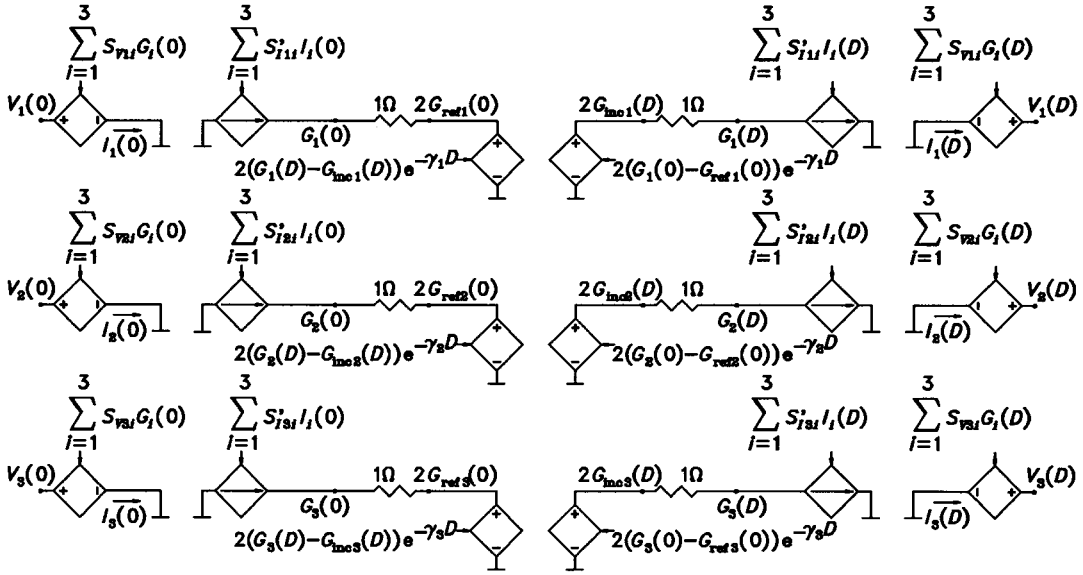

Fig. 4. A SPICE-compatible model for lossy lines based on the modal decoupling for $N = 3$.

Finally, it should be pointed out that there exist quite a few papers, dating from old ones up to recent ones (e.g., [10], [11]), where both the voltage- and current-wave equations are formulated and solved independently for one multiconductor transmission line. Such an analysis yields matrices $[\mathbf{S}_V]$ and $[\mathbf{S}_I]$ that are unrelated to each other, and subsequent computations are required to introduce a normalization so to satisfy (5). However, one must question the usefulness of solving two eigenvalue problems (except in theoretical investigations). The algorithm exposed in [6], which includes solving only one eigenvalue equation, is all that is needed to obtain all data for the present SPICE-compatible models without any normalization of the modal matrices. For a comprehensive treatment of this topic, see also [12].

The model of Fig. 3 was designed in [3] for the analysis of lossless multiconductor transmission lines. In recent versions of SPICE, there is a built-in model of simple lines with frequency-independent primary parameters L, C, R, and G. In conjunction with the model of Fig. 3, a lossy simple line can model the modal propagation assuming the modal attenuation coefficient to be independent of frequency. However, this is insufficient for most practical applications where the losses are frequency-dependent. To enable the analysis of lossy multiconductor transmission lines in the general case, one has to further modify the model of Fig. 3. One can make a hybrid of the models of Figs. 2 and 3, taking advantages of both of them. In the model of Fig. 2, the author has solved the problem of incorporating frequency variations of the modal attenuation coefficients and phase velocities by using the Laplace transform. On the other hand, for a large number of signal conductors (N), the scheme for the model of Fig. 3 looks simpler than for the model of Fig. 2. (The model of Fig. 3 contains more controlled generators, but fewer resistors than the model of Fig. 2.)

The resulting model is shown in Fig. 4. It can be visualized as the model of Fig. 3 where each simple transmission line is replaced by the model of Fig. 2 adapted for $N = 1$.

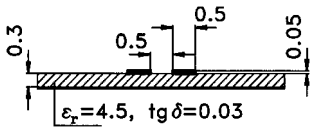

Fig. 5. Cross section of a symmetrical pair of microstrip lines. All dimensions are in millimeters.

This adaptation leaves two controlled voltage generators in the Laplace-transform domain and two "ordinary" controlled voltage generators. Each "ordinary" generator is controlled by the output of one generator in the Laplace-transform domain. Hence, each pair of controlled generators can be substituted by a single controlled voltage generator in the Laplace-transform domain, located in the middle of the scheme in Fig. 4. Each network of resistors that models the passive part of the Thévenin circuit in Fig. 2 reduces to a single resistor of resistance $1\,\Omega$, as shown in Fig. 4.

For the subcircuits of Figs. 2–4, augmentations may be needed to satisfy some requirements imposed by SPICE. First, if a transmission-line port is to be left open-circuited, in all models a "floating" node of a voltage generator would be obtained. The problem can be bypassed by including a resistor of a large resistance between each subcircuit terminal and ground. Second, if a transmission-line port is to be short-circuited or terminated in an inductor, for the models of Figs. 3 and 4, SPICE detects an illegal zero-resistance loop. To avoid this problem, a resistor of a small resistance can be included in series with each terminal. Finally, in the subcircuits generated for SPICE, the transmission-line ground can be made distinct from the common ground and the grounds at the two transmission-line ends can be mutually disconnected to allow modeling balanced lines.

V. Examples

Three examples are presented in this section. The first example is aimed at demonstrating how to implement the proposed

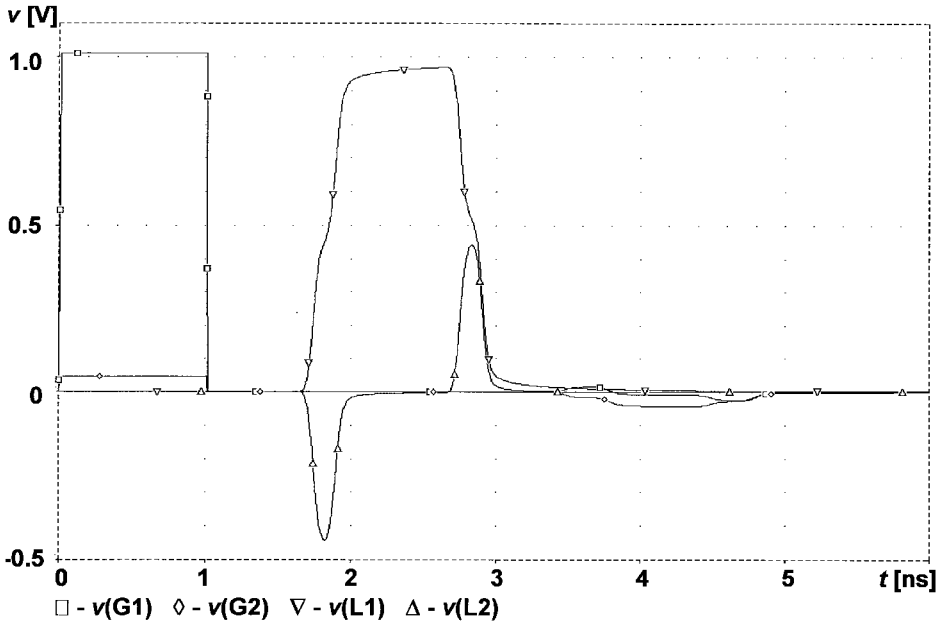

Fig. 6. Voltages of the coupled microstrip lines of Fig. 5 (excited by a pulse generator): voltage at the driven terminal (G1), near-end cross-talk (G2), transmitted signal (L1), and far-end cross-talk (L2).

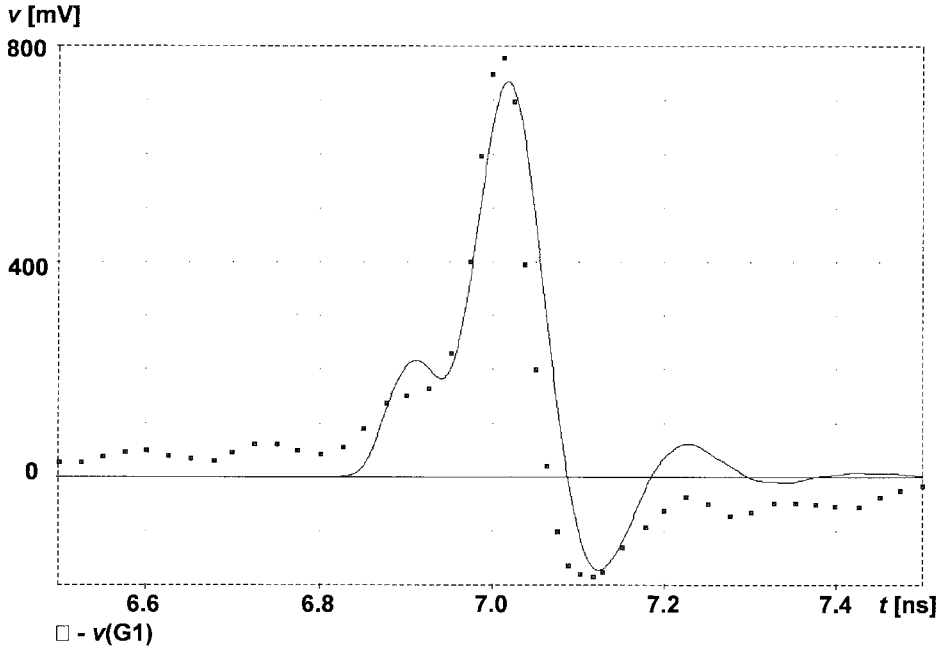

Fig. 7. Voltage of the input to a semirigid open-ended coaxial line (excited by a pulse generator): ——— theory, ■ ■ ■ experiment.

multiconductor transmission-line models with SPICE. The remaining two examples are aimed at comparing computed and measured data.

In the first example, consider the two symmetrical coupled microstrip lines sketched in Fig. 5. The substrate is 0.3-mm thick and its relative permittivity is 4.5. The loss tangent is 0.03 (at $f_{\rm ref} = 10$ GHz) and it is assumed to linearly increase with frequency. The conductivity of conductors is assumed to be $\sigma = 14$ mS/m. (This value is four times lower than the conductivity of copper so that it approximately models increased losses due to the surface roughness.) The conductor thickness is 50 μm, the width of each signal conductor is 0.5 mm, and the separation between them is 0.5 mm. The line length is 300 mm. One terminal of the line is driven against the ground by a pulse generator (of amplitude 2 V, zero rise time, and 1-ns duration) and 50-Ω internal resistance, while the three remaining terminals are connected to ground in 50-Ω resistors. The primary matrix parameters of the line were computed using the program of [13], for the reference

frequency $f_{\text{ref}} = 10$ GHz, and they are

$$[\mathbf{L}] = \begin{bmatrix} 307.4 & 41.3 \\ 41.3 & 307.4 \end{bmatrix} \frac{\text{nH}}{\text{m}}$$
$$[\mathbf{C}] = \begin{bmatrix} 117.5 & -5.8 \\ -5.8 & 117.5 \end{bmatrix} \frac{\text{pF}}{\text{m}}$$
$$[\mathbf{R}] = \begin{bmatrix} 93.50 & 9.69 \\ 9.69 & 93.50 \end{bmatrix} \frac{\Omega}{\text{m}}$$
$$[\mathbf{G}] = \begin{bmatrix} 192.6 & -3.0 \\ -3.0 & 192.6 \end{bmatrix} \frac{\text{mS}}{\text{m}}.$$

The two modes that can propagate along this line are the even and odd modes. The modal matrices evaluated by the same program (using the modal analysis in the frequency domain) are

$$[\mathbf{S}_V] = \begin{bmatrix} 0.7071 & -0.7071 \\ 0.7071 & 0.7071 \end{bmatrix} \text{V}$$
$$[\mathbf{S}_I] = \begin{bmatrix} 12.63 & -15.18 \\ 12.63 & 15.18 \end{bmatrix} \text{mA}.$$

(The imaginary parts of these matrices are about two orders of magnitude smaller and they are neglected.) The characteristic impedance matrix of the line is

$$[\mathbf{Z}_c] = \begin{bmatrix} 51.29 & 4.71 \\ 4.71 & 51.29 \end{bmatrix} \Omega.$$

The phase velocities of the even and odd mode are evaluated to be $c_{\phi 1} = 160.2$ mm/s and $c_{\phi 2} = 174.6$ mm/s, respectively. The parts of the modal attenuation coefficients due to the conductor losses (obtained by excluding the dielectric losses) are $\alpha_{c1} = 0.9214$ Np/m and $\alpha_{c2} = 0.8997$ Np/m, while the parts due to the dielectric losses (obtained by subtracting the conductor losses from the total losses) are $\alpha_{d1} = 5.296$ Np/m and $\alpha_{d1} = 4.543$ Np/m, respectively. Based on these data, a SPICE subcircuit of the form shown in Fig. 4 can easily be built, as given in the Appendix.

The time-domain response was computed using the SPICE version of [1] with the subcircuit of Fig. 4, but identical results are obtained with the subcircuit of Fig. 2. The ceiling of the time step in the transient analysis was taken to be 10 ps (as in the remaining examples presented in this section), and the final time 6 ns. After running for 18 s on a PC 486/100 (including reading and checking the circuit), the program resulted in voltages at the line terminals as shown in Fig. 6. Although the losses and the related dispersion are substantial, the computed response is causal. The plotted voltages are practically indistinguishable from results obtained by applying the inverse FFT to the frequency-domain response of the same line evaluated using the program of [8].

The second example is a simple semirigid coaxial cable. The diameter of the outer conductor is 2.985 mm and the diameter of the inner conductor is 0.9195 mm. The dielectric relative permittivity is 2.1, and its loss tangent is assumed to be 0.001 at 10 GHz and to vary linearly with frequency. The conductivity of the conductors is taken to be $\sigma = 16$ mS/m, based on measuring the cable attenuation as a function of frequency. The length of the cable is 718 mm, including two SMA connectors mounted on the cable. One end of the cable is connected to an HP 8510B network analyzer and the other end is left opened. The "pulse" response of the cable was measured setting the low-pass frequency to 20 GHz. The resulting reflected pulse is shown in Fig. 7 together with data computed using the model of Fig. 4. For the SPICE model, the primary parameters of the line were calculated using well-known closed-form formulas. The effects of discontinuities at the transition from the coaxial cable to the two SMA connectors were taken into account by 1.5-nH inductors located 4 mm from the cable ends. In the theoretical model, the electromotive force of the generator driving the line was taken as double the measured voltage reflected at the open test port of the network analyzer. With the final time of 8 ns, the run time of PSpice was 30 s. A good agreement between the theoretical and experimental results can be observed.

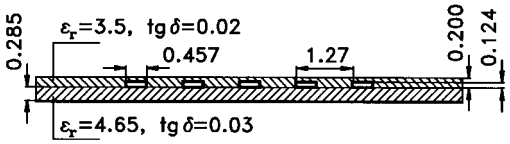

Fig. 8. Cross section of a microstrip transmission line with five signal conductors. All dimensions are in millimeters. (Reprinted from [6].)

The final example is the printed-circuit board described in [6]. The cross section of the board is shown in Fig. 8. The board has five traces of overall length 288 mm. The same conductivity is taken as in the previous example and the dielectric loss tangents (given in Fig. 8 at 10 GHz) are assumed to vary linearly with frequency. The line is driven by a 50-Ω step generator at one end of the leftmost signal conductor and the other ports are terminated in 50-Ω resistors to ground. The experimental results similar to those shown in [6] were obtained using a Tektronix 7854 sampling oscilloscope, an S52 pulse generator, and S4 and S6 sampling heads with a 50-ps step rise time [14]. For the SPICE model, the excitation waveform was taken by fitting the experimental data for the voltage at the driven port. The generator end of the multiconductor line had a flared part, which was modeled by a section 10-mm long with separations between the signal conductors increased to 2 mm. The final time for the transient analysis by PSpice was 5 ns, and the run time 61 s. Fig. 9 shows the simulated and experimental data for the voltages at selected ports. Again, a good agreement between the theoretical and experimental data can be observed. The differences between these two sets of results are, according to this experience, within the experimental errors and repeatability of the measured waveforms.

VI. Conclusion

Two novel SPICE-compatible models of multiconductor transmission lines are presented (Figs. 2 and 4) in this paper, built as subcircuits with controlled generators (some of them in the domain of the Laplace transform) and resistors. Both models can handle arbitrary lossy lines with frequency-dependent parameters, and can be used in SPICE to evaluate

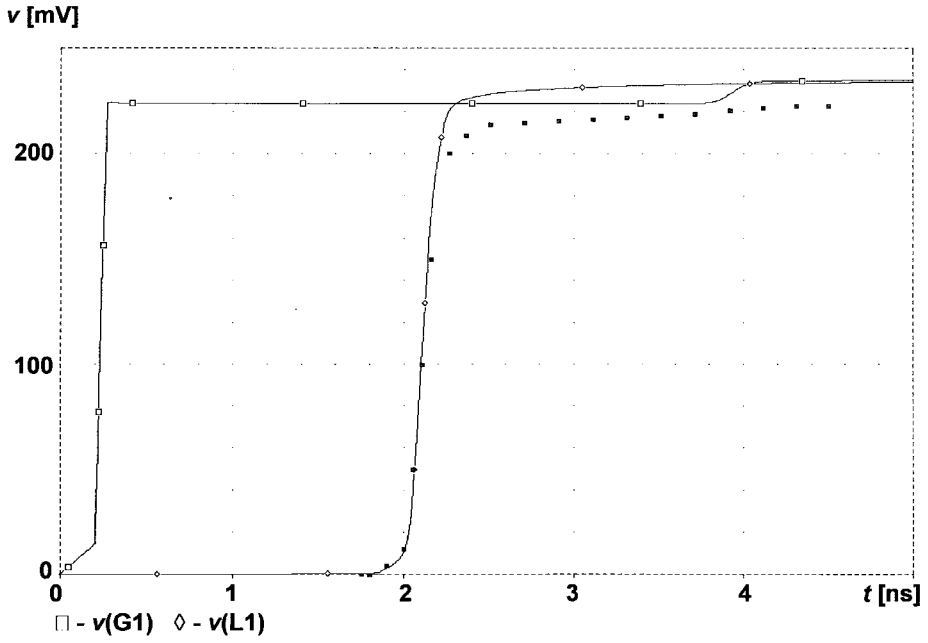

(a)

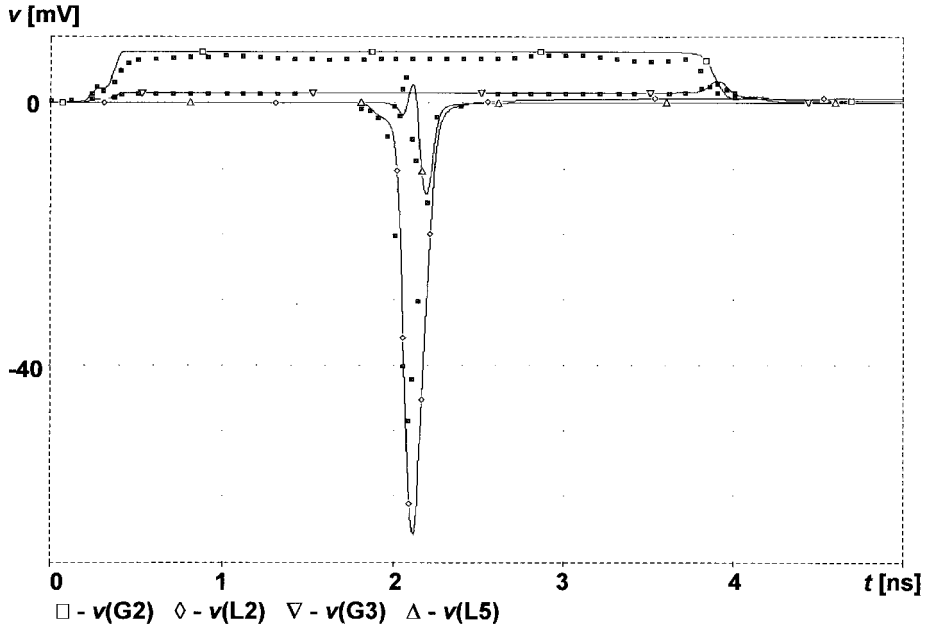

(b)

Fig. 9. Voltages at the terminals of the transmission line of Fig. 8 (excited by a step generator). The signal conductors are ordered from 1 (the driven, leftmost conductor) to 5 (the rightmost conductor). (a) Voltages at the generator (G1) and load end (L1) of the driven conductor and (b) voltages at the generator (G2) and load end (L2) of the second conductor, at the generator end of the third (middle) conductor (G3), and at the load end of the fifth conductor (L5): ——— theory, ■ ■ ■ experiment.

the frequency-domain and time-domain responses. This includes the impedance, admittance, and scattering parameters for multiport networks, when it is required to suitably drive and terminate the ports [8].

APPENDIX
EXAMPLE OF SPICE SUBCIRCUIT

An example of a SPICE subcircuit is shown below which corresponds to the first example in Section V. The subcircuit is for the model shown in Fig. 4, specialized for two signal conductors. This subcircuit was generated by the program of [5].

```
*
* SPICE PROGRAM NETLIST
*
.SUBCKT Line2
+ GNDG GNDL
+ UZG1 UZL1 UZG2 UZL2
+ PARAMS: LENGTH= 3.000E-01 W0= 6.284E+10
```

```
*
E_SG1 UG1 UGX1 POLY(2 )
+ UDLG1 GNDG UDLG2 GNDG
+ 0.0
+ 7.071E-01 7.071E-01
E_SL1 UL1 ULX1 POLY(2 )
+ UDLL1 GNDL UDLL2 GNDL
+ 0.0
+ 7.071E-01 7.071E-01
E_SG2 UG2 UGX2 POLY(2 )
+ UDLG1 GNDG UDLG2 GNDG
+ 0.0
+ -7.071E-01 7.071E-01
E_SL2 UL2 ULX2 POLY(2 )
+ UDLL1 GNDL UDLL2 GNDL
+ 0.0
+ -7.071E-01 7.071E-01
*
F_SG1 GNDG UDLG1 POLY(2 )
+ VF_G1 VF_G2
+ 0.0
+ 3.284E+01 -3.284E+01
F_SL1 GNDL UDLL1 POLY(2 )
+ VF_L1 VF_L2
+ 0.0
+ 3.284E+01 -3.284E+01
F_SG2 GNDG UDLG2 POLY(2 )
+ VF_G1 VF_G2
+ 0.0
+ 3.949E+01 3.949E+01
F_SL2 GNDL UDLL2 POLY(2 )
+ VF_L1 VF_L2
+ 0.0
+ 3.949E+01 3.949E+01
*
VF_G1 UGX1 GNDG 0V
VF_L1 ULX1 GNDL 0V
VF_G2 UGX2 GNDG 0V
VF_L2 ULX2 GNDL 0V
*
R_RL1 UDLG1 LL1 1
R_RL2 UDLG2 LL2 1
R_RR1 UDLL1 LR1 1
R_RR2 UDLL2 LR2 1
*
E_LAPL1 LL1 GNDG LAPLACE
+ {2*V(UDLL1 )-V(LR1 )-V(GNDL)}
+ {EXP(-LENGTH*SQRT((2* 8.997E-01*SQRT
+ (2*S/W0)+S/ 1.746E+08)/(2* 4.543E+00
+ /(W0*W0/ 1.746E+08/ 1.746E+08)+
+ 1.746E+08/S)))}
E_LAPR1 LR1 GNDL LAPLACE
+ {2*V(UDLG1 )-V(LL1 )-V(GNDG)}
+ {EXP(-LENGTH*SQRT((2* 8.997E-01*SQRT
+ (2*S/W0)+S/ 1.746E+08)/(2* 4.543E+00
+ /(W0*W0/ 1.746E+08/ 1.746E+08)+
+ 1.746E+08/S)))}
E_LAPL2 LL2 GNDG LAPLACE
+ {2*V(UDLL2 )-V(LR2 )-V(GNDL)}
+ {EXP(-LENGTH*SQRT((2* 9.214E-01*SQRT
+ (2*S/W0)+S/ 1.602E+08)/(2* 5.296E+00
+ /(W0*W0/ 1.602E+08/ 1.602E+08)+
+ 1.602E+08/S)))}
E_LAPR2 LR2 GNDL LAPLACE
+ {2*V(UDLG2 )-V(LL2 )-V(GNDG)}
+ {EXP(-LENGTH*SQRT((2* 9.214E-01*SQRT
+ (2*S/W0)+S/ 1.602E+08)/(2* 5.296E+00
+ /(W0*W0/ 1.602E+08/ 1.602E+08)+
+ 1.602E+08/S)))}
*
R_RSG1 UZG1 UG1 1E-9
R_RPG1 UZG1 GNDG 1E+9
R_RSL1 UZL1 UL1 1E-9
R_RPL1 UZL1 GNDL 1E+9
R_RSG2 UZG2 UG2 1E-9
R_RPG2 UZG2 GNDG 1E+9
R_RSL2 UZL2 UL2 1E-9
R_RPL2 UZL2 GNDL 1E+9
*
.ENDS
```

The subcircuit has six external nodes: GNDG (ground for the generator end of the line), GNDL (ground for the load end), UZG1 (signal conductor #1 at the generator end), UZL1 (signal conductor #1 at the load end), UZG2 (signal conductor #2 at the generator end), and UZL2 (signal conductor #2 at the load end). Two parameters are defined: the line length (0.3 m) and the reference angular frequency ($\omega_0 = 2\pi f_{\text{ref}} = 6.284 \cdot 10^{10}$ s^{-1}). E_SG1, E_SL1, E_SG2, and E_SL2 are the controlled voltage generators in Fig. 4, at the far left and right sides. The coefficients in their control functions are elements of the matrix $[\mathbf{S}_V]$. F_SG1, F_SL1, F_SG2, and F_SL2 are the controlled current generators in Fig. 4. The coefficients in their control functions are elements of the matrix $[\mathbf{S}_I]^{-1}$, and the currents correspond to the dummy voltage generators VF_G1, VF_L1, VF_G2, and VF_L2.

E_LAPL1, E_LAPR1, E_LAPL2, and E_LAPR2 are the controlled voltage generators in the Laplace-transform domain. The exponential terms in their control functions correspond to (19) and (20). Finally, 1-nΩ resistors are connected in series and 1-GΩ resistors in parallel with the subcircuit external nodes to satisfy SPICE requirements if the nodes are left opened or shorted to ground.

ACKNOWLEDGMENT

The author wishes to thank his students Darko Cvetković and Goran Ćujić, for skillfully building SPICE subcircuits for multiconductor transmission lines.

REFERENCES

[1] *PSpice Version 5.2*, MicroSim Co., Irvine, CA, 1992.
[2] V. K. Tripathy and J. B. Rettig, "A SPICE model for multiple coupled microstrips and other transmission lines," *IEEE Trans. Microwave Theory Tech.*, vol. MTT-33, pp. 1513–1518, Dec. 1985.
[3] L. Carin and K. J. Webb, "An equivalent circuit model for terminated hybrid mode multiconductor transmission lines," *IEEE Trans. Microwave Theory Tech.*, vol. 37, pp. 1784–1793, Nov. 1989.

[4] V. K. Tripathy and A. Hill, "Equivalent circuit modeling of losses and dispersion in single and coupled lines for microwave and millimeter-wave integrated circuits," *IEEE Trans. Microwave Theory Tech.*, vol. 36, pp. 256–262, Feb. 1988.
[5] A. R. Djordjević, D. D. Cvetković, G. M. Ćujić, T. K. Sarkar, and M. B. Baždar, *MULTLIN for Windows: Circuit-Analysis Models for Multiconductor Transmission Lines, Software and User's Manual*, Norwood, MA: Artech House, 1996.
[6] A. R. Djordjević, T. K. Sarkar, and R. F. Harrington, "Time-domain response of multiconductor transmission lines," *Proc. IEEE*, vol. 75, pp. 743–764, June 1987.
[7] A. R. Djordjević, T. K. Sarkar, R. F. Harrington, and M. B. Baždar, *Time-Domain Response of Multiconductor Transmission Lines, Software and User's Manual*. Norwood, MA: Artech House, 1989.
[8] A. R. Djordjević, M. B. Baždar, G. M. Vitošević, T. K. Sarkar, and R. F. Harrington, *Scattering Parameters of Microwave Networks with Multiconductor Transmission Lines, Software and User's Manual*. Norwood, MA: Artech House, 1989.
[9] T. R. Arabi, A. T. Murphy, T. K. Sarkar, R. F. Harrington, and A. R. Djordjević, "On the modeling of conductor and substrate losses in multiconductor, multidielectric transmission line systems," *IEEE Trans. Microwave Theory Tech.*, vol. 39, pp. 1090–1097, July 1991.
[10] K. D. Marx, "Propagation modes, equivalent circuits, and characteristic terminations for multiconductor transmission lines with a nonhomogeneous dielectric medium," *IEEE Trans. Microwave Theory Tech.*, vol. MTT-21, pp. 450–457, July 1973.
[11] G. G. Gentili and M. Salazar-Palma, "The definition and computation of modal characteristic impedance in quasi-TEM coupled transmission lines," *IEEE Trans. Microwave Theory Tech.*, vol. 43, pp. 338–343, Feb. 1995.
[12] G.-T. Lei, G.-W. Pan, and B. K. Gilbert, "Examination, clarification, and simplification of modal decoupling method for multiconductor transmission lines," *IEEE Trans. Microwave Theory Tech.*, vol. 43, pp. 2090–2100, Sept. 1995.
[13] A. R. Djordjević, M. B. Baždar, R. F. Harrington, and T. K. Sarkar, *LINPAR for Windows: Matrix Parameters for Multiconductor Transmission Lines, Software and User's Manual*. Norwood, MA: Artech House, 1995.
[14] T. R. Arabi, M. Manela, T. K. Sarkar, and A. R. Djordjević, "Theoretical/Experimental Determination of Crosstalk in Multiconductor Transmission Lines," Syracuse Univ., ECE Dept., Microwave Lab., Syracuse, New York, Internal Rep.

Antonije R. Djordjević was born in Belgrade, Yugoslavia, on April 28, 1952. He received the B.Sc., M.Sc., and D.Sc. degrees from the School of Electrical Engineering, University of Belgrade, Yugoslavia, in 1975, 1977, and 1979, respectively.

In 1975 he joined the School of Electrical Engineering, University of Belgrade, as a Teaching Assistant. He was promoted to an Assistant Professor, Associate Professor, and Professor, in 1982, 1988, and 1992, respectively. In 1983, he was a Visiting Associate Professor at Rochester Institute of Technology, Rochester, NY. Since 1992, he has also been an Adjunct Associate Professor with Syracuse University, Syracuse, NY. His main area of interest is numerical electromagnetics, in particular applied to multiconductor transmission lines, wire and surface antennas, and electromagnetic-compatibility problems.